organoids

MDPI

Communication

Development of Low-Cost CNC-Milled PMMA Microfluidic Chips as a Prototype for Organ-on-a-Chip and Neurospheroid Applications

Sushmita Mishra, Ginia Mondal and Murali Kumarasamy *

Department of Biotechnology, National Institute of Pharmaceutical Education and Research (NIPER), Hajipur, Export Promotion Industrial Park (EPIP), Vaishali 844102, Bihar, India

* Correspondence: muralik@niperhajipur.ac.in or drmuralinano@gmail.com; Tel.: +91-6224-277224 or +91-6224-277226 or +91-6224-277229

Abstract: Improved in vitro models are needed to reduce costs and delays in central nervous system (CNS) drug discovery. The FDA Modernization Acts 2.0 and 3.0 require human-centered alternative testing methods to mitigate animal-based experiments and discovery delays, and to ensure human safety. Developing cost-efficient, flexible microfluidic chips is essential to advance organ-on-chip (OoC) technology for drug discovery and disease modeling. While CNC micromilling shows promise for fabricating microfluidic devices, it remains underutilized due to limited accessibility. We present a simple CNC-milled flexible microfluidic chip fabricated from thermoplastic poly (methyl methacrylate) (PMMA). The structure of the microplate included drilled openings for connecting the wells. The chip's biocompatibility was evaluated with isolated primary neuronal cultures from postnatal Wistar rat pups (p1). Primary cells cultured in the device showed high viability, differentiation, and 3D neurosphere formation, similar to conventional well-plate cultures. Neuronal cultures showed neurite growth and functional markers. Although cleanroom-based methods provide higher accuracy, the chip effectively promotes cell viability, differentiation, and alignment, offering an ideal platform for tissue modeling and OoC applications. It allows cell biologists to quickly create prototypes at lower cost and in less time than required for soft lithography and is a viable alternative to the current manufacturing methods.

Keywords: computer numerical control (CNC) machine; organ-on-a-chip; micromilling; primary neural cells; 3D neurospheroid

check for updates

Academic Editor: Süleyman Ergün

Received: 14 March 2025
Revised: 1 June 2025
Accepted: 9 June 2025
Published: 11 June 2025

Citation: Mishra, S.; Mondal, G.; Kumarasamy, M. Development of Low-Cost CNC-Milled PMMA Microfluidic Chips as a Prototype for Organ-on-a-Chip and Neurospheroid Applications. *Organoids* **2025**, *4*, 13. https://doi.org/10.3390/organoids4020013

Copyright: © 2025 by the authors. Licensee MDPI, Basel, Switzerland. This article is an open access article distributed under the terms and conditions of the Creative Commons Attribution (CC BY) license (https://creativecommons.org/licenses/by/4.0/).

1. Introduction

In the central nervous system (CNS), drug discovery and disease modeling, animal experiments are used to predict pharmacodynamics and toxicity. However, the drawbacks and limitations of traditional in vivo and in vitro Transwell systems are increasingly recognized, as they often fail to adequately replicate the human physiological environment. The FDA Modernization Act 2.0 passed in December 2022, and on 6 February 2024, the FDA Modernization Act 3.0 was introduced with the aim of minimizing and replacing the use of animals. Therefore, there is an urgent need for alternative models providing accurate data to improve drug development. Approval of the FDA Modernization Act 2.0 and 3.0 has allowed the pharmaceutical industry to expand its research methods, including alternative models such as [1,2] microphysiological systems (MPS) or organ-on-chip (OoC) technology designed to recapitulate the structure and functions of human organs

by combining different living cells in a 3D, physiological environment in small fluid devices. Microfluidics offers new opportunities in cell biology, particularly for understanding cell-to-cell communication and the pathophysiology of CNS diseases in vitro, as well as for evaluating novel therapies [3,4]. The properties of liquids at the microscale are useful for MPS, allowing the creation of cell culture models that better mimic actual physiology compared to traditional static culture systems [5,6]. Advancing the development of OoC systems requires rapid, simple, straightforward, and cost-effective fabrication technologies. Current methods often depend on micro-/nano-fabrication techniques such as lithography and PDMS casting, which require multiple steps, are expensive, and require clean room conditions [7]. In recent developments, 3D printing, along with stereolithography or digital light processing (DLP) printers using photoresins, has reduced the fabrication time and costs associated with microfluidic devices. However, organic solvents used in cleaning and the cytotoxicity of some resins may make these devices less suitable for culturing fragile cells, such as primary stem cells and primary cells. To support CNS drug discovery while reducing animal testing, more relevant cell culture models that maintain microplate-based throughput compatibility are needed [8–12].

Microfluidic chips serve as emerging human pathophysiologically relevant in vitro models for conducting a variety of cell and tissue cultures, such as 2D, 3D, and organotypic cultures [13]. Cells in 2D culture conditions lose their traits, but in 3D culture, cell–cell and cell–extracellular matrix (ECM) interactions allow cells to develop similarly to in vivo phenotypes [14–16]. Neurospheroids from primary cells maintain key features of neural tissue, including cell interactions, matrix dynamics, and organization, which are essential for studying neural development and neural network activity [17]. These 3D models effectively replicate the pathological features of neurodevelopmental and neurodegenerative diseases, including amyloid aggregation, synaptic dysfunction, and glial activation [18,19]. Microfluidics is now linked to 3D cell culture because it helps improve the structure and function of cells in controlled environments [20,21]. Microfluidics can replicate the in vivo environment of cells by providing micro-scale complex structures and carefully precise conditions. The integration of 3D cell culture and microfluidic technology holds significant potential for applications similar to real tissues, like the new OoC system [22]. Conventional microfabrication methods like soft lithography, injection molding, and 3D printing have limitations. Soft lithography requires cleanroom facilities and skilled labor, which are often unavailable in biological labs [23]. Xurography offers a cost-effective solution; however, it lacks precision and is limited in feature size, making it unsuitable for applications requiring high fabrication accuracy or complex 3D microchannel structures [24]. Thus, cleanroom-free, cost-effective, and simple design alternatives like CNC milling are essential for OoC research and rapid prototyping capabilities [25–27]. CNC milling is advantageous for microfluidic device manufacturing, either by fabricating the entire device or creating molds for polymer casting, facilitating PDMS-based microfluidic devices for biomedical applications. Therefore, our study investigated the CNC milling properties of a low-cost, intuitive milling platform and demonstrated its application to microfluidic device development. It provides precision and versatility for micro-scale components. In this proof-of-concept study, we investigate the feasibility of these approaches using CNC milling [9,10]. In this preliminary study, we have developed CNC-milled flexible PMMA microfluidic chips that can be fabricated with a precision of less than 10–20 µm. Additionally, high optical transparency can be achieved through surface treatments for microscopic applications [23,28], which facilitates the cultivation of primary neuronal cells and their differentiation, as well as the formation of 3D neurospheres, and evaluates their immunocytochemical characteristics. It represents a significant advancement in the devel-

opment of more design-flexible, cost-effective, and reliable OoC prototypes for CNS drug discovery applications.

2. Materials and Methods

2.1. Microfluidic Chip Design and Fabrication

Microfluidic chips are produced using CNC milling techniques. All CNC-milled parts were fabricated with a CNC milling machine—5axis UX600, Quaser for engraving the microchannels and microfeatures (patterned on microdevices) of PMMA chips. In this study, we used PMMA because of its optical transparency, elasticity, biocompatibility, and gas permeability. Feeds, speeds, and milling strategies were kept uniform between the mills and were selected based on previous work by Guckenberg et al. [29]. PMMA sheets with a thickness of 2.5 mm were utilized for mold fabrication. The micromilling Unigraphix NX 12 software served as the computer-aided manufacturing (CAM) program to convert the CAD files into a numerical control (NC) programming language (G-code file) for operating the CNC micromill (Figure 1A) [30,31]. The microfluidic chip, which consists of three main chambers, was designed, and the three chambers were further connected by permeable channels to allow a gradient flow of liquids (Figure 1B). The choice of materials must be carefully considered to meet predefined system requirements. The basis for this is a multi-layered approach that takes into account the following aspects: physiological significance, biocompatibility, physical and mechanical characteristics, design complexity, cost, scalability, and compatibility with existing chip fabrication methods [32–34]. Therefore, polymethyl methacrylate (PMMA) was deemed a suitable carrier for producing the chip.

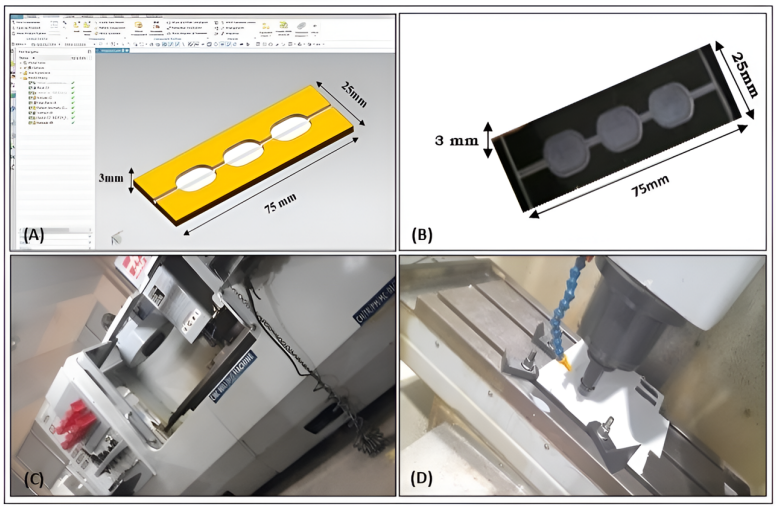


Figure 1. Characterization of microfluidic chip. (**A**) Microfluidic chip designed in Unigraphix NX 12 Software. (**B**) PMMA- based prototype design made by CNC. (**C**) CNC milling machine. (**D**) Nozzle of CNC.

2.2. Animals

Primary Neuronal Culture

Primary neurons were prepared from Wistar rat pups' (p1) cortical tissues according to the animal experimentation license (NIPER-H/IAEC/28/22), issued by the IAEC of NIPER Hajipur. First, rat pups (p1) were cleaned with alcohol and sacrificed by decapitation with small surgical scissors and placed in a 60 mm tissue culture Petri dish (Catalog No 960020, Tarson, Kolkata, India) containing cold PBS [35–37]. The meninges were peeled after removal of the animal's olfactory bulbs and the remaining subcortical components, both the left and right hemispheres, were utilized. Cortices were digested with Collagenase/Dispase® (Catalog No COLLDISP-RO, Roche, Basel, Switzerland) dis-

solved in DMEM (Catalog No 10566016, Gibco, Thermo Scientific, Waltham, MA, USA) to a final concentration of 1 mg/mL by incubating at 37 °C for 5 min. Cells were mechanically dissociated by pipetting 5–10 times until homogeneous, filtered through a 40 µm Corning® cell strainer (Catalog No CLS431750-50EA, Corning, New York, NY, USA), and centrifuged at 1500 rpm for 3 min. Isolated cell suspensions were reconstituted in neuronal media comprising DMEM, 5% v/v heat-inactivated Fetal Bovine Serum (FBS) (Catalog No A3160801, Gibco, Thermo Scientific, Waltham, MA, USA), and 1% v/v Antibiotic-Antimycotic (100×) (Catalog No 15240062, Gibco, Thermo Scientific, Waltham, MA, USA). The cells were seeded at a density of 10^6 cells/cm^2 onto 20 µg /mL poly-L-lysine (PLL) hydrobromide (Catalog No P6282, Sigma, Taufkirchen, Germany) coated 6-well plates (Catalog No 980010, Tarson, Kolkata, India) and cultured for 2 days (DIV2).

2.3. Culturing Primary Neurons in Microfluidic Chips

Microfluidic chips were sterilized with UV (60 min), 70% Ethanol (Catalog No 1009831011, EMSURE®, Merck, Darmstadt, Germany), and washed with sterile PBS, pH 7.4 (Catalog No 10010023, Gibco, Thermo Scientific, Waltham, MA, USA). The microfluidic chip was coated with 20 µg/mL PLL for 30 min at 37 °C. with 5% CO_2 to enhance cell adhesion. The chips were then completely rinsed with PBS to remove the PLL and air dried in a biosafety cabinet. Primary neuronal culture DIV 2 was centrifuged at 1500 rpm for 3 min and resuspended in neuronal culture media. The cells were seeded at 2×10^5 cells onto a PLL-coated microfluidic chip, placed in a 60 mm culture dish and incubated at 37 °C, 5% CO_2, and 95% humidity for 48 h before imaging and metabolic assays.

2.4. Three-Dimensional Culture on a Chip

Complete serum-free media was prepared with Neurobasal Medium (1×) (Catalog No 10888022, Gibco, Thermo Scientific, Waltham, MA, USA), DMEM/F-12 (1×) (Catalog No 11320082, Gibco, Thermo Scientific, Waltham, MA, USA), B-27 Supplement Minus Vitamin A (1×) (Catalog No 12587010, Gibco, Thermo Scientific, Waltham, MA, USA), and 1% *v/v* Antibiotic-Antimycotic (100×) (Catalog No 15240062, Gibco, Thermo Scientific, Waltham, MA, USA). The primary neuronal culture DIV 2 was centrifuged at 1500 rpm for 3 min and resuspended in serum-free media. Primary cortical cells (2×10^5) were suspended in 1 mL serum-free neuron-specific medium and plated onto a microfluidic chip. The chips were placed in a 60 mm culture dish at 37 °C, 5% CO_2, and 95% humidity. After 48 h, 3D neurospheres on DIV4 that reached ~100 µm diameter were used for imaging, live–dead assays, Fluo-4 AM staining, and fixed with 4% paraformaldehyde (PFA) (Catalog No P6148, Sigma, Taufkirchen, Germany) for 30 min. They were washed 3 times to remove residual PFA, and stored samples were submerged in PBS at 4 °C until use. A few 3D neurospheres generated inside a microfluidic chip (DIV 4) were transferred to a microfluidic chip and 6-well plate (control) coated with PLL and cultured in neuronal media for 3 days (DIV 7) and fixed with PFA for 30 min, then washed 3 times to remove residual PFA and stored in PBS at 4 °C until use.

2.5. Determination of Cell Viability

2.5.1. Two-Dimensional Cell Viability

Cell viability was assessed by live DNA staining with Hoechst, a cell-permeant blue fluorescent stain for nuclear staining. After 48 h, the neuronal medium was removed, and the cell-loaded chip was washed with PBS. Hoechst (33342, trihydrochloride trihydrate) (Catalog No H1399, Invitrogen™, Thermo Scientific, Waltham, MA, USA) was added at 5 µM at 37 °C for 20 min. The chip was washed with PBS and observed under a fluorescence microscope (Carl Zeiss Axio Vert.A1, Carl Zeiss Microscopy GmbH, Jena, Germany), with images analyzed using Zeiss software ZEN (version 3.8).

2.5.2. Three-Dimensional Neurospheroid Viability

Neurospheres are free-floating 3D spheroids that are cultured in vitro and contain neural progenies that can differentiate into neurons, glial cells, and other neural tissue cell types. The neurospheroids were removed from the chip along with the serum-free medium in a 0.5 mL Eppendorf tube. After 5–10 min, the medium was removed and washed with PBS. Hoechst (5 μM) was added to neurospheroid for 20 min at 37 °C, washed with PBS and observed under a Confocal microscope (Nikon AX/AX R, Nikon Instruments Inc., Melville, NY, USA) on a 35 mm μ-dish (Catalog No 81156, ibidi, Gräfelfing, Germany).

2.6. Fluo-4 AM Calcium Staining

2.6.1. Two-Dimensional Primary Neuronal Culture Staining with Fluo-4 AM

Cell-permeable Ca^{2+} indicator (Fluo-4 AM), emits green fluorescence when it penetrates the membranes of living cells. After 48 h, the neuronal medium was removed, and the chip was washed with PBS. Cells were incubated with Fluo-4 AM (Catalog No F14201 Invitrogen™, Thermo Scientific, Waltham, MA, USA) at 5 μM in PBS at 37 °C for 20 min, washed with PBS, and observed under a fluorescence microscope (Carl Zeiss Axio Vert.A1).

2.6.2. Three-Dimensional Neurospheroid Staining with Fluo-4 AM

Three-dimensional neurospheres are stained with Fluo-4 AM to study calcium signaling in relation to neural activity and differentiation. The neurospheroids were removed with serum-free medium in a 0.5 mL Eppendorf tube. After washing with PBS, Fluo-4 AM was added at 5 μM concentration, incubated for 20 min at 37 °C, washed with PBS, and observed under a fluorescence microscope. Images were analyzed using Zeiss software ZEN (version 3.8).

2.6.3. Immunocytochemistry of Neurospheres

The 3D neurospheroids generated from the microfluidic chip after 48 h (DIV 4) and the neurospheres differentiated on the microfluidic chip (DIV 7) were washed with PBS permeabilized with 0.1% Triton X-100 made in PBS solution PBS (PBT) for 15 min, washed 3 times with PBS and blocked with 2% BSA for 1 h, and washed 3 times with PBB (PBS + 0.5% BSA). This was followed by incubation with 1st primary antibody for overnight at 4 °C and being washed 3 times with PBB. It was incubated with secondary antibody at room temperature for 1 h, washed 3 times with PBB, and blocked with 2% BSA for 1 h and further washed 3 times with PBB. It was incubated with 2nd primary antibody overnight at 4 °C and washed 3 times with PBB. Following incubation with secondary antibody at room temperature for 1 h, it was counterstained with Fluoroshield™ with DAPI (Catalog No F6057, Sigma, Taufkirchen, Germany) onto an ibidi dish and a microfluidic chip. The primary antibodies used for the 3D neurospheroids included iba1 (1:1000, Catalog No PA5-27436, Thermofisher Scientific), MAP2 (1:1000, Catalog No ab288714, Abcam, Cambridge, UK), GFAP (1:1000, Catalog No sc-33673, Santa Cruz, Dallas, TX, USA), β-III Tubulin (1:1000, Catalog No sc-51670, Santa Cruz, Dallas, TX, USA), Nestin (1:1000, Sigma-Aldrich, Catalog No N5413, Sigma, Taufkirchen, Germany). The secondary antibodies used included Goat Anti-Rabbit IgG H&L (Alexa Fluor® 647) (1:1000, Catalog No ab150083, Abcam, Cambridge, UK), Goat Anti-Rabbit IgG H&L (Alexa Fluor® 488) (1:1000, Catalog No ab150077, Abcam, Cambridge, UK), Goat Anti-Mouse IgG H&L (Alexa Fluor® 647) (1:1000, Catalog No ab150115, Abcam, Cambridge, UK), m-IgGκ BP-CFL 488 (1:1000, Catalog No sc-51617610, Santa Cruz, Dallas, TX, USA). The primary antibodies used for the differentiated neurospheres included Nestin (1:1000), GFAP (1:1000). The secondary antibodies used included Goat Anti-Rabbit IgG H&L (Alexa Fluor® 488) (1:1000, Catalog No ab150077, Abcam,

Cambridge, UK) and Goat Anti-Mouse IgG H&L (Alexa Fluor® 647) (1:1000, Catalog No ab150115, Abcam, Cambridge, UK).

3. Results

3.1. Characterization of Microfluidic Chips

Fabrication of the 3D-PMMA Chips

CNC micromilling was used for micro-machining of PMMA sheets (Figure 1A,D). Building on these findings, we developed CNC micro-machined flexible microfluidic chips for cell culture applications (Figure 1A–C). The fabrication process involves several sequential steps. In micromilling, a 0.3 mm nozzle mill was used. Spindle speed ranged from 10,000 to 24,000 rpm, with a feed rate of 60 mm/min and a 100 µm cutting depth. Before micromilling, the PMMA sheet's protective film was removed, and the tip of the cutting end mill was kept at zero via a touch sensor on the top of the PMMA [38].

When cutting, appropriate lubrication or cooling is required to prevent overheating and material damage. After fabricating, the chip was incubated in 70% ethanol for 5 min for sterilization and washed with PBS [39]. Surface roughness in OoC devices affects cell distribution and optical transparency, which is essential for imaging. The fabrication procedure made it possible to create channels with a low surface roughness without the need for additional chemical or physical treatment to improve the surface quality [40]. In this way, we were able to produce a polymer-based microfluidic device and a cost-effective prototype design without a clean room. It can create prototypes quickly and provides a one-step process for cost-effectively creating features at multiple scales. Once fabrication is complete, the microfluidic device is tested and validated for assessing the biocompatibility of the chips [41]. This microfluidic device was constructed using three main chambers that serve as a compartment: three oval wells seeded with cells embedded in a poly-L-lysine (PLL)-coated polymer. They are connected by channels [42]. The characterization was carried out using inverted microscopy. The milled chips showed consistent channel structures with smooth cross-sections, confirming successful fabrication. The chip specifications were as follows: length = 75 mm; width = 25 mm, and depth = 3 mm, as presented in Figure 1A,B.

The microfabrication of the chip was performed using PMMA, which is inexpensive and has good biocompatibility. The fabrication technique involved in production of the chip was a CNC milling machine, which is inexpensive and is cleanroom-free. It consists of three major compartments that are interconnected. The channels enable the flow of fluid, simulating the circulation of nutrients, oxygen, and signaling molecules in the brain cells and allowing us to study various neurological diseases and test potential treatments. The characterization of the chip was carried out using inverted microscopy (Figure 1B) and a vernier caliper. It is crucial to specify the details of the microfluidic chip design, which is essential for connecting microchannels and microchambers. The chip specifications are as follows: length = 75 mm; width = 25 mm, and depth = 3 mm, as presented in Figure 1A,B.

3.2. Attachment and Neurite Growth in 2D and 3D Form of Primary Neuronal Cells in the Microfluidic Chip

To evaluate the microfluidic chips' feasibility and biocompatibility with primary neurons, we isolated and cultured them within the fabricated chip. The cerebral cortex was isolated from the p-0-1 Wistar rats' brains, as shown in Figure 2A,B and the cells from cortical regions Figure 2A–C of p-0-1 Wistar rats were isolated. The meninges were removed and then dissociated into single cells and cultured into neuronal media, as shown in Figure 2D. Primary neuronal culture was observed after 48 h, consisting of single cells with few cell clusters, as shown in Figure 2E.

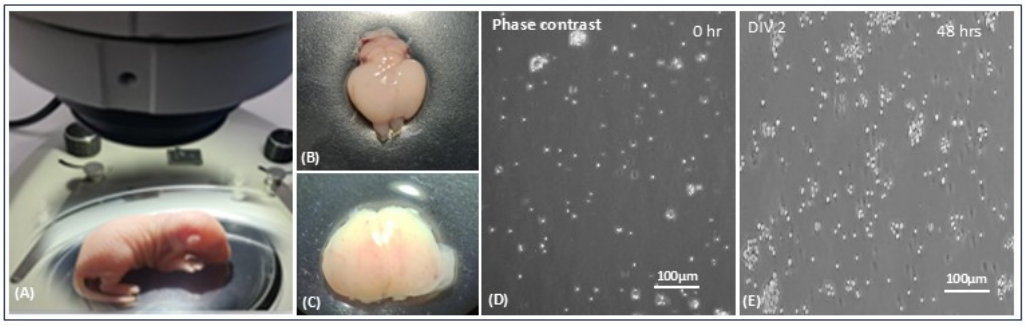


Figure 2. Isolation of primary cortical cells. (**A**) Brain of p-0-1 Wistar rat pup. (**B**,**C**) Brain cortex of p-0-1 Wistar rat pup. (**D**) Phase-contrast image of dissociated primary neuronal culture observed at DIV 0. (**E**) Phase-contrast image of primary neuronal culture observed at DIV 2.

Bright-field microscopy images of cells after 48 h of culturing demonstrated cellular growth in both the chamber and channel of the microfluidic chip shown in Figure 3A–H. The primary neuronal culture was uniformly grown throughout the microfluidic chip, as depicted in Figure 3A–D. Three-dimensional spheres of varying sizes were formed after 48 h of culture in serum-free media within the chamber of the microfluidic chip, as illustrated in Figure 3E–H. These results indicate that the 2D and 3D cultures were well-maintained in the microfluidic chip.

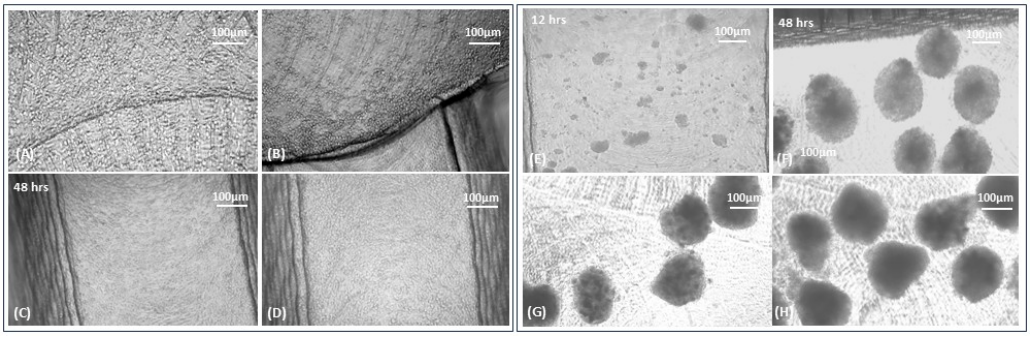


Figure 3. Growth of 2D cells and 3D neurospheroids on a microfluidic chip. (**A**–**D**) Primary neuronal cells cultured for 48 h in neuronal media. (**E**) Primary neuronal cells cultured for 12 h in serum-free media showed the emergence of small neurospheres. (**F**–**H**) After 48 h, neurospheres were observed with a clear boundary and translucent appearance. Images were captured at 10× magnification, scale bar: 100 µm.

3.2.1. Neurospheres' Size Distribution

Neurospheres of Different Sizes Were Generated from the Microfluidic Chip

Figure 4 and Supplementary Figure S1, shows the variation in sizes of neurospheres grown for 48 h on the microfluidic chip Supplementary Figure S2. Statistical analyses were performed using 320 GraphPad Prism version 8.42 for Windows (GraphPad Software, Inc.). A one-way ANOVA was performed to compare measurements between the primary neurospheres between 50 and 100 µm, 100 and 150 µm, and >150 µm (Supplementary Figure S3A). The average number of neurospheres between 50 and 100 µm is 88.13 ± 0.64, 100–150 µm is equal to 124.2 ± 1.6, and the number of neurospheres that were greater than 150 µm in size was 153.6 ± 0.8 (N = 3 experiments; M = 2 replicates). Statistical analysis using Tukey's multiple comparisons between 50 and 100 µm vs. 100 and 150 µm and 50 and 100 µm vs. >150 µm yielded highly significant results ($p < 0.0001$), while the difference between 100 and 150 µm and >150 µm was also statistically significant ($p = 0.0002$). These findings indicate a non-uniform size distribution and suggest that neurosphere growth under the given culture conditions favors the formation of medium-sized

structures, with a few neurospheres also achieving larger diameters. To assess the relative distribution of neurospheres by size, the mean percentage of neurospheres in each group was compared using one-way ANOVA, and revealed a significant overall difference among groups ($p < 0.0001$) (Supplementary Figure S3B). Post hoc analysis using Tukey's multiple comparisons test demonstrated that the percentage of neurospheres in the 50–100 µm group (49.5%) was significantly higher than in both the 100–150 µm group (42.9%; $p < 0.0001$) and the >150 µm group (7.6%; $p < 0.0001$). The difference between the 100 and 150 µm and >150 µm groups was also statistically significant ($p < 0.0001$). These findings indicate a non-uniform size distribution and suggest that small neurospheres grow inside the microfluidic chip in 48 h, with a small proportion of larger neurospheres.

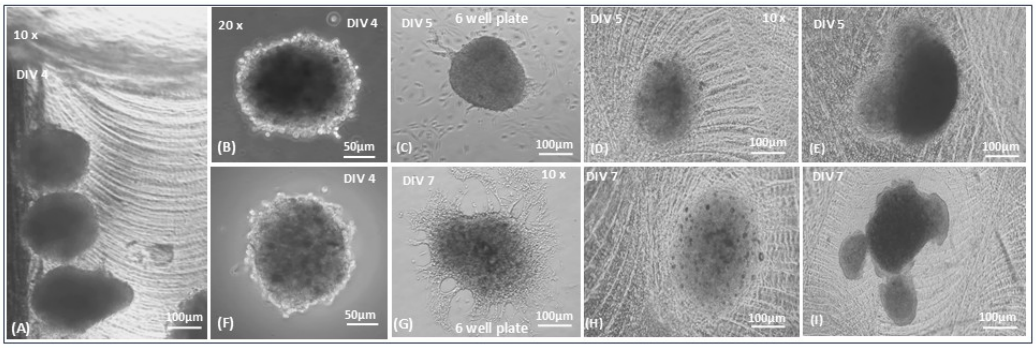


Figure 4. Morphological features of 3D neurospheroids. (**A**) Three-dimensional neurospheroids formed after 48 h on a microfluidic chip (DIV 4). (**B**,**F**) Floating neurospheres from microfluidic chip were collected on a 35 mm µ-dish (ibidi) for microscopy. Neurospheres were observed with a clear boundary and a translucent appearance. Images were captured at 20× magnification, scale bar: 50 µm. (**C**,**G**) Neurospheres were cultured for (DIV 5) and 72 h (DIV 7) in neuronal (serum) media in a 6-well plate, showing very clear and distinct neurite growth with the appearance of microspikes. (**D**,**H**) Neurospheres cultured for 48 h and 72 h, respectively, in neuronal (serum) media in a microfluidic chip. Large round cells were observed with no visible distinct microspikes. (**E**,**I**) Neurospheres, when cultured for 48 h (DIV 5), showed merging of 2 neurospheres, and 72 h (DIV 7) showed merging of 4 neurospheres, respectively, in neuronal (serum) media in a microfluidic chip. Images were captured at 10× magnification, scale bar: 100 µm.

3.2.2. Neurosphere Differentiation

Figure 4A shows the floating culture of neurospheres of variable sizes inside the microfluidic chip. This heterogeneity likely results from the passive aggregation mechanism under static conditions and slight differences in the microenvironment across the device. Figure 4B,F show young, healthy neurospheres from a microfluidic chip observed in an ibidi dish. Figure 4C,G show neurospheres attached to the bottom of the plate, and beginning to differentiate in 6-well plate with microspikes. This indicates neurite outgrowth, a key indicator of neuronal differentiation and functional development. Figure 4D,H show a neurosphere attached to the bottom of the microfluidic chip, beginning to differentiate without visible microspikes. It may be due to the geometry and optical properties of the chip (e.g., channel depth, material thickness, and light refraction) that high-resolution imaging is limited, especially in deeper regions where neurites extended beyond a single focal plane. Considering this limitation, we propose design modifications in future iterations, such as thinner channel floors, optical-grade substrates, or incorporation of neurite-guiding structures, to enable accurate neurite outgrowth measurement. Figure 4E,I depict the chances of neurospheres merging during the culture. While neurosphere merging may contribute to heterogeneity in size, it also offers advantages such as enhanced cell–cell signaling, improved maturation potential, and increased cell numbers for downstream

analysis. In developmental models, merged neurospheres may better mimic in vivo like 3D architecture and morphogenic processes.

3.3. Two-Dimensional and Three-Dimensional Cell Viability

Following 48 h of incubation, the microfluidic chip with primary neuronal cells stained with Hoechst (5 µM) was examined. It was observed that Hoechst successfully stained the primary neuronal cells, as shown in Figure 5A,B, indicating cellular viability over the 48 h incubation period. This finding suggests that this design is suitable for long-term experiments. The microfluidic chip exhibited compatibility with primary mixed neuronal cells. The 3D spheres were stained with Hoechst, as depicted in Figure 5E,F, demonstrating the excellent compatibility of the microfluidic chip for 3D cell culture, which is suitable for drug and toxicity screening studies.

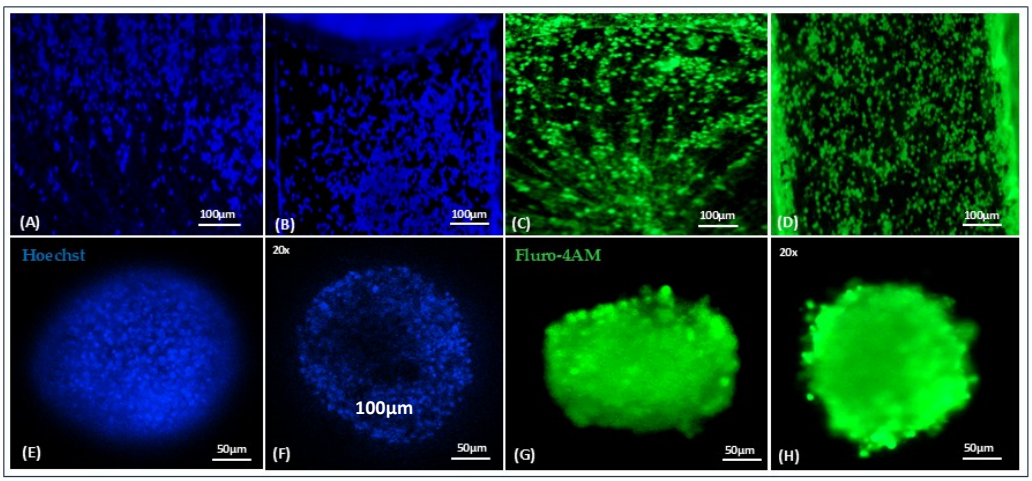


Figure 5. Hoechst and Fluo-4 AM staining of 2D cells and 3D neurospheroids on a chip. (**A**,**B**) Two-dimensional cells inside the microfluidic chip stained with Hoechst (5 µM) for 20 min showed intact nuclei in all cells, indicating complete viability. (**E**,**F**) Three-dimensional neurospheroids of the microfluidic chip stained with Hoechst (5 µM) for 20 min. Fluorescence microscopy revealed strong, uniform fluorescence in all cells, indicating successful dye loading and confirming that the overall cell population was viable under the experimental conditions. (**C**,**D**) Two-dimensional cells inside the microfluidic chip stained with Fluo-4 AM (5 µM) for 20 min. (**G**,**H**) Three-dimensional neurospheroids of the microfluidic chip stained with Fluo-4 AM (5 µM) for 20 min. Images were captured at 20× magnification, scale bar: 50 µm.

3.4. Fluo-4 AM Staining

After 48 h of incubation, primary neuronal cells and 3D neurospheres on the microfluidic chip were stained with Fluo-4 AM (5 µM) and subsequently observed. Fluo-4 AM staining of primary neuronal culture, as shown in Figure 5C,D and Supplementary Figure S2, and 3D neurospheres, as shown in Figure 5G,H, provides signatures of intracellular calcium activity, suggesting the usage of the microfluidic chip for metabolic assays.

3.5. Immunocytochemical Characterization of Neurospheres

The immunostaining of fixed floating neurospheres on a microfluidic chip was stained with primary antibodies against GFAP (astrocytes), Nestin (neural progenitors), βIII-tubulin (immature neurons), MAP2 (mature neurons), and IBA1 (microglia), followed by fluorescently conjugated secondary antibodies. Nuclei were counterstained with DAPI and observed under a Confocal microscope (Nikon AX/AX R). The neurospheres contain cells positive for neural stem/progenitor markers Nestin (red), the neuronal marker β III Tubulin (green), glial markers GFAP (red), microglia marker IBA1(green), and neuronal dendrites MAP2 (red), as shown in (Supplementary Figure S4). Fluorescent signals were analyzed to

identify and localize the expression of neural lineage markers. GFAP and IBA1 staining indicated glial populations, while Nestin highlighted undifferentiated progenitor cells. βIII-tubulin and MAP2 staining were used to assess early and mature neuronal differentiation, respectively. Representative images show distinct expression patterns of neural and glial lineage markers, confirming the multipotency and differentiation potential of neurosphere-derived cells. The presence of MAP2+ cells alongside Tuj1+ cells indicates progression from immature to more differentiated neurons.

3.6. Immunocytochemical Characterization of Differentiated Neurosphere

Neurospheres were differentiated via plating onto a PLL-coated microfluidic chip and cultured under differentiation conditions for 3 days. Differentiation of 3D neurospheres on the microfluidic chip was characterized by assessing marker expression using GFAP (red) and Nestin (green) staining, with nuclei counterstained using DAPI (blue) and visualized under a fluorescence microscope (Carl Zeiss Axio Vert.A1) as shown in (Supplementary Figure S5). Nestin, a neural stem/progenitor cell marker, was robustly expressed throughout the neurosphere, indicating a predominance of undifferentiated cells. GFAP, a marker of astrocytic lineage commitment, was detected in a subset of cells, suggesting the initiation of glial differentiation within the population. Cells inside the neurospheres and cells emigrating from the spheres were stained positive for the neural progenitor marker Nestin (green). GFAP (red) demonstrates early heterogeneity, comprising undifferentiated progenitors and glial-committed precursors.

4. Discussion

We chose PMMA because of its positive features, such as its ease of fabrication, high optical transparency, excellent mechanical properties, and biocompatibility [43,44]. Fast, cost-effective methods for OoC models are essential for drug discovery and disease modeling [40]. We demonstrate that transparent PMMA enables one-step fabrication of flexible microfluidic devices through CNC milling. The water contact angle of PMMA is 70.0°, indicating moderate hydrophobicity, biocompatibility, and specific cell adhesion properties, making it a suitable material for observing cell behavior and creating complex microfluidic devices for cell biological studies [45]. To determine optimal conditions for fabricating a microfluidic PMMA device for mammalian cell culture and OoC applications, we designed channel compartments that were precisely milled [46,47]. We fabricated a microfluidic chip with three chambers, fabricated using CNC milling. The chip specifications were as follows: length = 75 mm; width = 25 mm, and depth = 3 mm, as presented in Figure 1A,B. In addition, the channels of the cell culture are connected to the intake and output reservoirs, which are connected to subsequent chambers, ensuring a continuous nutrient supply to other chambers in the case of other types of cells. We tested the CNC-milled microfluidic chip by culturing primary neuronal culture and evaluating their biocompatibility over a 2-day period, and structural organization compared to conventional 2D and 3D culture systems. Interestingly, primary neuronal cultures cultured in the microfluidic chip exhibited good cell viability, and its spheres formed in the presence of serum-free cell culture medium. This suggests that the fabricated microfluidic chip supports neuronal cell growth and enhances 3D cell self-assembly in serum-free medium. Primary dissociated neuronal cultures and their derived 3D spheres serve as tools for CNS disease modeling, therapeutics, and neurotoxicological studies [37,48]. The 3D neurospheroids were developed within the microfluidic chips, and cell viability was confirmed through live staining. We used Fluo-4 AM to characterize the functional activity of neurons, glia, and other cells by their calcium signals [49,50]. During the culture period, we observed occasional merging of adjacent neurospheroids within the microfluidic chamber, particularly under static condi-

tions where limited fluid movement and confined geometry may facilitate contact between spheroids. This merging can lead to an increase in spheroid size and introduce variability in size distribution. Such variability may influence experimental outcomes, including cell differentiation, viability, and neurite outgrowth, as larger spheroids are known to exhibit different internal gradients of oxygen, nutrients, and signaling molecules. While this represents a limitation in terms of assay standardization, it may also offer advantages in certain contexts by promoting enhanced cell–cell interactions and better mimicking aspects of in vivo neural tissue development. Future iterations of the device could incorporate micropatterned features or fluidic barriers to prevent fusion and maintain spheroid uniformity. The 3D spheroids showed neurite outgrowth, indicating functional differentiation of neuronal cells, while maintaining high viability markers. The immunocytochemical analysis of neurospheres provided key insights into the cellular composition and lineage differentiation potential of neural stem/progenitor cells (NSPCs) cultured in serum-free media in a microfluidic chip. The expression patterns of GFAP, Nestin, βIII-Tubulin, MAP2, and IBA1 demonstrate that the neurospheres contain a heterogeneous population of cells, which are capable of differentiating into major neural lineages—neurons, astrocytes, and potentially microglia. These findings confirm the multipotency of neurosphere-derived NSPCs and their utility as a model for studying neurogenesis, gliogenesis, and potential therapeutic applications in neuroregenerative medicine. The immunocytochemical analysis of differentiated neurospheres revealed distinct populations of GFAP- and Nestin-positive cells, reflecting both lineage commitment and residual progenitor identity within the culture. The presence of GFAP-positive cells indicates successful differentiation of a subset of cells toward an astrocytic lineage, consistent with previous findings that neural stem/progenitor cells (NSPCs) within neurospheres are capable of generating glial cells under differentiation-promoting conditions. GFAP expression is a hallmark of astrocyte maturation, and its localization throughout the adherent neurosphere culture confirms astrocytic differentiation as part of the natural lineage progression in vitro. The coexistence of GFAP+ astrocytes and Nestin+ progenitors highlights the multipotency and plasticity of NSPCs within neurospheres. The fabricated microfluidic chip supports primary neuronal cultures, promotes neurite outgrowth, maintains cell viability, and supports key marker expression, making it promising for CNS disease modeling (Organoids and OoC) and drug testing [51–63]. Although the study demonstrated the chip's feasibility for primary neurons in both 2D and 3D under static conditions, future integration of flow-perfusion systems could enhance media distribution and better replicate physiological conditions. The static structure successfully supported cell viability and differentiation, demonstrating the chip's robustness. Future research could investigate applications in CNS drug testing and disease modeling. Our approach provides a reliable, simple, and cost-effective cell culture model.

5. Conclusions

We developed a microfluidic chip using CNC milling with PMMA, supporting primary neuronal culture and 3D neurospheroids. Both 2D and 3D cultures showed high viability comparable to well plate cultures, with 3D spheres forming neurites and expressing functional markers. CNC micromilling presents a low-cost, accessible, and flexible alternative for fabricating microfluidic devices. These features make it advantageous for academic labs seeking a balance between precision, affordability, and prototyping speed. CNC fabrication provides a platform for cell culture and OoC applications. Future work will address flow perfusion for CNS drug discovery and neurodegenerative models.

Limitations of the Study

In our microfluidic chip system, fluorescent imaging provided better clarity than Bright-field microscopy, with structural features like neurite extensions, astrocytic processes, or microglial branches are more readily observed using fluorescence due to their high signal-to-noise ratio and specific labeling. Static culture conditions can limit nutrient and oxygen exchange, potentially affecting long-term cell viability and mimicking of physiological conditions. We note that future designs may incorporate dynamic perfusion to better replicate in vivo environments. While we demonstrated that CNC-machined chip surfaces express structural and functional proteins of primary neurons in 2D and 3D, their higher surface roughness limits cell attachment and growth. We use CNS-fabricated chips as master molds with PDMS curing for smoother surfaces. Injection molding provides high reproducibility and scalability for mass production. Our approach, by contrast, is better suited to rapid prototyping and small-batch production, although with reduced dimensional precision compared to industrial-grade injection molding. Soft lithography requires multiple fabrication steps. In contrast, our CNC-based approach allows for faster prototyping.

Supplementary Materials: The following supporting information can be downloaded at: https://www.mdpi.com/article/10.3390/organoids4020013/s1, Figure S1: A-P. Neurospheres generated inside microfluidic chip; Figure S2: Staining of 2D cells on Microfluidic chip; Figure S3: Size of primary 3D neurospheres generated from the microfluidic chip; Figure S4: Immunocytochemical characterization of neurospheres generated from the microfluidic chip stained with lineage-specific markers; Figure S5: Immunocytochemical characterization of neurospheres differentiated on the microfluidic chip.

Author Contributions: Conceptualization, S.M. and M.K.; methodology, G.M. and S.M.; software, G.M.; validation, S.M., G.M. and M.K.; formal analysis, S.M. and G.M.; investigation, S.M.; resources, M.K.; data curation, M.K. and S.M.; writing—original draft preparation, M.K.; writing—review and editing, G.M. and S.M.; visualization, M.K.; supervision, M.K.; project administration, M.K.; funding acquisition, M.K. All authors have read and agreed to the published version of the manuscript.

Funding: This study was supported by the Department of Pharmaceuticals (DoP), Ministry of Chemicals and Fertilizers (MoCF), Government of India (GoI), and the Center of Excellence (CoE) in Biological Therapeutics, NIPER Hajipur, for the development of advanced in vitro models and the Common Research program (CRP) of all NIPERs; Promotion of Research and Innovation in Pharma (PRIP) MedTech Sector (56014/1/2023-NIPER (E - 25511))

Institutional Review Board Statement: The animal study protocol was approved by the Institutional Review Board (or Ethics Committee) of NIPER Hajipur (NIPER-H/IAEC/28/22 on 17 October 2022).

Informed Consent Statement: Not applicable.

Data Availability Statement: We share research data upon request.

Acknowledgments: We thank Jayita S for her initial support. We thank CIPET | Department of Chemicals and Petrochemicals, MoCF, GoI, for access to their CNC machine facilities. We are also gratefully acknowledging the Confocal-Nikon-STORM Imaging facility at NIPER Hajipur for providing access to the confocal scanning microscopy Nikon-STORM Imaging facility.

Conflicts of Interest: The authors declare no conflicts of interest. The funders had no role in the study design, data collection, analysis, manuscript writing, or publication decisions.

References

1. Carratt, S.A.; Zuch de Zafra, C.L.; Oziolor, E.; Rana, P.; Vansell, N.R.; Mangipudy, R.; Vaidya, V.S. An industry perspective on the FDA Modernization Act 2.0/3.0: Potential next steps for sponsors to reduce animal use in drug development. *Toxicol. Sci.* **2024**, *203*, 28–34. [CrossRef] [PubMed]
2. Han, J.J. FDA Modernization Act 2.0 allows for alternatives to animal testing. *Artif. Organs* **2023**, *47*, 449–450. [CrossRef] [PubMed]

3. Sanapathi, J.; Vipparthi, P.; Mishra, S.; Sosnik, A.; Kumarasamy, M. Microfluidics for brain endothelial cell-astrocyte interactions. *Organs Chip* **2023**, *5*, 100033. [CrossRef]
4. Osaki, T.; Shin, Y.; Sivathanu, V.; Campisi, M.; Kamm, R.D. In vitro microfluidic models for neurodegenerative disorders. *Adv. Healthc. Mater.* **2018**, *7*, 1700489. [CrossRef]
5. Wang, Y.I.; Carmona, C.; Hickman, J.J.; Shuler, M.L. Multiorgan microphysiological systems for drug development: Strategies, advances, and challenges. *Adv. Healthc. Mater.* **2018**, *7*, 1701000. [CrossRef]
6. Young, A.T.; Deal, H.; Rusch, G.; Pozdin, V.A.; Brown, A.C.; Daniele, M. Simple design for membrane-free microphysiological systems to model the blood-tissue barriers. *Organs Chip* **2023**, *5*, 100032. [CrossRef]
7. Sen, A.K.; Raj, A.; Banerjee, U.; Iqbal, S.R. Soft lithography, molding, and micromachining techniques for polymer micro devices. *Microfluid. Electrophor. Methods Protoc.* **2019**, *1906*, 13–54.
8. Singh, G.; Mishra, A.; Mathur, A.; Shastri, S.; Nizam, A.; Rizwan, A.; Dadial, A.S.; Firdous, A.; Hassan, H. Advancement of organ-on-chip towards next generation medical technology. *Biosens. Bioelectron.* **2024**, *18*, 100480. [CrossRef]
9. Tajeddin, A.; Mustafaoglu, N.J.M. Design and fabrication of organ-on-chips: Promises and challenges. *Micromachines* **2021**, *12*, 1443. [CrossRef]
10. Yen, D.P.; Ando, Y.; Shen, K.J.T. A cost-effective micromilling platform for rapid prototyping of microdevices. *Technology* **2016**, *4*, 234–239. [CrossRef]
11. Khoo, H.; Allen, W.S.; Arroyo-Currás, N.; Hur, S.C. Rapid prototyping of thermoplastic microfluidic devices via SLA 3D printing. *Sci. Rep.* **2024**, *14*, 17646. [CrossRef] [PubMed]
12. Balázs, B.Z.; Geier, N.; Takács, M.; Davim, J.P. A review on micro-milling: Recent advances and future trends. *Int. J. Adv. Manuf. Technol.* **2021**, *112*, 655–684. [CrossRef]
13. Guo, Q.R.; Zhang, L.L.; Liu, J.F.; Li, Z.; Li, J.J.; Zhou, W.M.; Wang, H.; Li, J.Q.; Liu, D.Y.; Yu, X.Y.; et al. Multifunctional microfluidic chip for cancer diagnosis and treatment. *Nanotheranostics* **2021**, *5*, 73. [CrossRef]
14. Tehranirokh, M.; Kouzani, A.Z.; Francis, P.S.; Kanwar, J.R. Microfluidic devices for cell cultivation and proliferation. *Biomicrofluidics* **2013**, *7*, 51502. [CrossRef]
15. El-Ali, J.; Sorger, P.K.; Jensen, K.F. Cells on chips. *Nature* **2006**, *442*, 403–411. [CrossRef]
16. Feng, X.; Du, W.; Luo, Q.; Liu, B.F. Microfluidic chip: Next-generation platform for systems biology. *Anal. Chim. Acta* **2009**, *650*, 83–97. [CrossRef]
17. Lancaster, M.A.; Knoblich, J.A. Organogenesis in a dish: Modeling development and disease using organoid technologies. *Science* **2014**, *345*, 1247125. [CrossRef]
18. Choi, S.H.; Kim, Y.H.; Hebisch, M.; Sliwinski, C.; Lee, S.; D'Avanzo, C.; Chen, H.; Hooli, B.; Asselin, C.; Muffat, J.; et al. A three-dimensional human neural cell culture model of Alzheimer's disease. *Nature* **2014**, *515*, 274–278. [CrossRef]
19. Raja, W.K.; Mungenast, A.E.; Lin, Y.T.; Ko, T.; Abdurrob, F.; Seo, J.; Tsai, L.H. Self-organizing 3D human neural tissue derived from induced pluripotent stem cells recapitulate Alzheimer's disease phenotypes. *PloS ONE* **2016**, *11*, e0161969. [CrossRef]
20. Wang, Z.; He, X.; Qiao, H.; Chen, P. Global trends of organoid and organ-on-a-chip in the past decade: A bibliometric and comparative study. *Tissue Eng. Part* **2020**, *26*, 656–671. [CrossRef]
21. Dutta, D.; Heo, I.; Clevers, H. Disease modeling in stem cell-derived 3D organoid systems. *Trends Mol. Med.* **2017**, *23*, 393–410. [CrossRef] [PubMed]
22. Li, X.; Valadez, A.V.; Zuo, P.; Nie, Z. Microfluidic 3D cell culture: Potential application for tissue-based bioassays. *Bioanalysis* **2012**, *4*, 1509–1525. [CrossRef] [PubMed]
23. Scott, S.M.; Ali, Z. Fabrication Methods for Microfluidic Devices: An Overview. *Micromachines* **2021**, *12*, 319. [CrossRef] [PubMed]
24. Liu, X.; Sun, A.; Brodský, J.; Gablech, I.; Lednický, T.; Vopařilová, P.; Zítka, O.; Zeng, W.; Neužil, P. Microfluidics chips fabrication techniques comparison. *Sci. Rep.* **2024**, *14*, 28793. [CrossRef]
25. Ahmed, M.A.; Jurczak, K.M.; Lynn Jr, N.S.; Mulder, J.P.S.; Verpoorte, E.M.; Nagelkerke, A. Rapid prototyping of PMMA-based microfluidic spheroid-on-a-chip models using micromilling and vapour-assisted thermal bonding. *Sci. Rep.* **2024**, *14*, 2831. [CrossRef]
26. Carter, S.S.D.; Atif, A.R.; Kadekar, S.; Lanekoff, I.; Engqvist, H.; Varghese, O.P.; Tenje, M.; Mestres, G. PDMS leaching and its implications for on-chip studies focusing on bone regeneration applications. *Organs Chip* **2020**, *2*, 100004. [CrossRef]
27. Nasiri, R.; Zhu, Y.; de Barros, N.R. Microfluidics and Organ-on-a-Chip for Disease Modeling and Drug Screening. *Biosensors* **2024**, *14*, 86. [CrossRef]
28. Becker, H.; Gärtner, C. Polymer microfabrication methods for microfluidic analytical applications. *Electrophor. Int. J.* **2000**, *21*, 12–26. [CrossRef]
29. Guckenberger, D.J.; De Groot, T.E.; Wan, A.M.; Beebe, D.J.; Young, E.W. Micromilling: A method for ultra-rapid prototyping of plastic microfluidic devices. *Lab Chip* **2015**, *15*, 2364–2378. [CrossRef]

30. Behroodi, E.; Latifi, H.; Bagheri, Z.; Ermis, E.; Roshani, S.; Salehi Moghaddam, M. A combined 3D printing/CNC micro-milling method to fabricate a large-scale microfluidic device with the small size 3D architectures: An application for tumor spheroid production. *Sci. Rep.* **2020**, *10*, 22171. [CrossRef]
31. Ding, P.; Huang, X. Huang, and Machines, Sustainable optimization of micro-milling machining parameters considering reliability assessment. *Mech. Based Des. Struct. Mach.* **2025**, *53*, 864–901. [CrossRef]
32. Kawakita, S.; Mandal, K.; Mou, L.; Mecwan, M.M.; Zhu, Y.; Li, S.; Sharma, S.; Hernandez, A.L.; Nguyen, H.T.; Maity, S.; et al. Organ-on-a-chip models of the blood–brain barrier: Recent advances and future prospects. *Small* **2022**, *18*, 2201401. [CrossRef] [PubMed]
33. Nielsen, A.V.; Beauchamp, M.J.; Nordin, G.P.; Woolley, A.T. 3D printed microfluidics. *Annu. Rev. Anal. Chem.* **2020**, *13*, 45–65. [CrossRef] [PubMed]
34. Fardous, R.S.; Alshmmari, S.; Tawfik, E.; Khadra, I.; Ramadan, Q.; Zourob, M. An integrated and modular compartmentalized microfluidic system with tunable electrospun porous membranes for epithelialized organs-on-a-chip. *ACS Appl. Mater. Interfaces* **2024**, *16*, 40767–40786. [CrossRef]
35. Beaudoin III, G.M.; Lee, S.H.; Singh, D.; Yuan, Y.; Ng, Y.G.; Reichardt, L.F.; Arikkath, J. Culturing pyramidal neurons from the early postnatal mouse hippocampus and cortex. *Nat. Protoc.* **2012**, *7*, 1741–1754. [CrossRef]
36. Pozzi, D.; Ban, J.; Iseppon, F.; Torre, V. An improved method for growing neurons: Comparison with standard protocols. *J. Neurosci. Methods* **2017**, *280*, 1–10. [CrossRef]
37. Petrović, A.; Ban, J.; Tomljanović, I.; Pongrac, M.; Ivaničić, M.; Mikašinović, S.; Mladinic, M. Establishment of long-term primary cortical neuronal cultures from neonatal opossum Monodelphis domestica. *Front. Cell. Neurosci.* **2021**, *15*, 661492. [CrossRef]
38. Cao, U.M.; Zhang, Y.; Chen, J.; Sayson, D.; Pillai, S.; Tran, S.D. Microfluidic organ-on-a-chip: A guide to biomaterial choice and fabrication. *Int. J. Mol. Sci.* **2023**, *24*, 3232. [CrossRef]
39. Sarkar, T.; Nguyen, T.; Moinuddin, S.M.; Stenmark, K.R.; Nozik, E.S.; Saha, D.; Ahsan, F. A protocol for fabrication and on-chip cell culture to recreate PAH-afflicted pulmonary artery on a microfluidic device. *Micromachines* **2022**, *13*, 1483. [CrossRef]
40. Arandian, A.; Bagheri, Z.; Ehtesabi, H.; Najafi Nobar, S.; Aminoroaya, N.; Samimi, A.; Latifi, H. Optical imaging approaches to monitor static and dynamic cell-on-chip platforms: A tutorial review. *Small* **2019**, *15*, 1900737. [CrossRef]
41. Huh, D.; Kim, H.J.; Fraser, J.P.; Shea, D.E.; Khan, M.; Bahinski, A.; Hamilton, G.A.; Ingber, D.E. Microfabrication of human organs-on-chips. *Nat. Protoc.* **2013**, *8*, 2135–2157. [CrossRef] [PubMed]
42. Marie, R.; Beech, J.P.; Vörös, J.; Tegenfeldt, J.O.; Höök, F. Use of PLL-g-PEG in micro-fluidic devices for localizing selective and specific protein binding. *Langmuir* **2006**, *22*, 10103–10108. [CrossRef] [PubMed]
43. Chen, Y.; Zhang, L.; Chen, G. Fabrication, modification, and application of poly (methyl methacrylate) microfluidic chips. *Electrophoresis* **2008**, *29*, 1801–1814. [CrossRef]
44. Xu, J.; Locascio, L.; Gaitan, M.; Lee, C.S. Room-temperature imprinting method for plastic microchannel fabrication. *Anal. Chem.* **2000**, *72*, 1930–1933. [CrossRef]
45. Nielsen, J.B.; Hanson, R.L.; Almughamsi, H.M.; Pang, C.; Fish, T.R.; Woolley, A.T. Microfluidics: Innovations in materials and their fabrication and functionalization. *Anal. Chem.* **2019**, *92*, 150–168. [CrossRef]
46. Tevlek, A.; Kecili, S.; Ozcelik, O.S.; Kulah, H.; Tekin, H.C. Spheroid engineering in microfluidic devices. *ACS Omega* **2023**, *8*, 3630–3649. [CrossRef]
47. Chen, Q.; Wang, Y. The application of three-dimensional cell culture in clinical medicine. *Biotechnol. Lett.* **2020**, *42*, 2071–2082. [CrossRef]
48. Sammoura, F.M.; Popova, D.; Morris, A.; Hart, R.P.; Richardson, J.R. Methods for shipping live primary cortical and hippocampal neuron cultures from postnatal mice. *Curr. Res. Neurobiol.* **2023**, *4*, 100069. [CrossRef]
49. Chen, Y.; Huang, L.M. A simple and fast method to image calcium activity of neurons from intact dorsal root ganglia using fluorescent chemical Ca^{2+} indicators. *Mol. Pain* **2017**, *13*, 1744806917748051. [CrossRef]
50. İpek, Ö.Y.; Abbas, F.; Sajidy, H.; Canepari, M. Fast Neuronal Calcium Signals in Brain Slices Loaded with Fluo-4 AM Ester. *Eur. J. Neurosci.* **2025**, *61*, e16657. [CrossRef]
51. Cho, A.N.; Jin, Y.; An, Y.; Kim, J.; Choi, Y.S.; Lee, J.S.; Kim, J.; Choi, W.Y.; Koo, D.J.; Yu, W.; et al. Microfluidic device with brain extracellular matrix promotes structural and functional maturation of human brain organoids. *Nat. Commun.* **2021**, *12*, 4730. [CrossRef] [PubMed]
52. Saorin, G.; Caligiuri, I.; Rizzolio, F. Microfluidic organoids-on-a-chip: The future of human models. *Semin. Cell Dev. Biol.* **2023**, *144*, 41–54. [CrossRef] [PubMed]
53. Salmon, I.; Grebenyuk, S.; Fattah, A.R.A.; Rustandi, G.; Pilkington, T.; Verfaillie, C.; Ranga, A. Engineering neurovascular organoids with 3D printed microfluidic chips. *Lab Chip* **2022**, *22*, 1615–1629. [CrossRef]
54. Seiler, S.T.; Mantalas, G.L.; Selberg, J.; Cordero, S.; Torres-Montoya, S.; Baudin, P.V.; Ly, V.T.; Amend, F.; Tran, L.; Hoffman, R.N.; et al. Modular automated microfluidic cell culture platform reduces glycolytic stress in cerebral cortex organoids. *Sci. Rep.* **2022**, *12*, 20173. [CrossRef]

55. Tsai, Y.C.; Ozaki, H.; Morikawa, A.; Shiraiwa, K.; Pin, A.P.; Salem, A.G.; Phommahasay, K.A.; Sugita, B.K.; Vu, C.H.; Mamoun Hammad, S.; et al. Proof of concept for brain organoid-on-a-chip to create multiple domains in forebrain organoids. *RSC Adv.* **2025**, *15*, 3749–3755. [CrossRef]
56. Kandra, M.; Vanova, T.; Jongen, V.A.; Pospíšil, J.; Novák, J.; Chochola, V.; Buryška, T.; Prokop, Z.; Hodný, Z.; Hampl, A.; et al. A closed 3D printed microfluidic device for automated growth and differentiation of cerebral organoids from single-cell suspension. *Biotechnol. J.* **2024**, *19*, e2400240. [CrossRef]
57. Ao, Z.; Cai, H.; Havert, D.J.; Wu, Z.; Gong, Z.; Beggs, J.M.; Mackie, K.; Guo, F. One-Stop Microfluidic Assembly of Human Brain Organoids to Model Prenatal Cannabis Exposure. *Anal. Chem.* **2020**, *92*, 4630–4638. [CrossRef]
58. Papamichail, L.; to Koch, L.S.; Veerman, D.; Broersen, K.; van der Meer, A.D. Organoids-on-a-chip: Microfluidic technology enables culture of organoids with enhanced tissue function and potential for disease modeling. *Front. Bioeng. Biotechnol.* **2025**, *13*, 1515340. [CrossRef]
59. Abdulla, A.; Chen, S.; Chen, Z.; Wang, Y.; Yan, H.; Chen, R.; Ahmad, K.Z.; Liu, K.; Yan, C.; He, J.; et al. Three-dimensional microfluidics with dynamic fluidic perturbation promotes viability and uniformity of human cerebral organoids. *Biosens. Bioelectron.* **2023**, *240*, 115635. [CrossRef]
60. Zhu, Y.; Zhang, X.; Sun, L.; Wang, Y.; Zhao, Y. Engineering Human Brain Assembloids by Microfluidics. *Adv. Mater.* **2023**, *35*, e2210083. [CrossRef]
61. Wang, Z.; Zhang, Y.; Li, Z.; Wang, H.; Li, N.; Deng, Y. Microfluidic Brain-on-a-Chip: From Key Technology to System Integration and Application. *Small* **2023**, *19*, e2304427. [CrossRef] [PubMed]
62. Saglam-Metiner, P.; Yildirim, E.; Dincer, C.; Basak, O.; Yesil-Celiktas, O. Humanized brain organoids-on-chip integrated with sensors for screening neuronal activity and neurotoxicity. *Mikrochim. Acta.* **2024**, *191*, 71. [CrossRef] [PubMed]
63. Teli, P.; Kale, V.; Vaidya, A. Beyond animal models: Revolutionizing neurodegenerative disease modeling using 3D in vitro organoids, microfluidic chips, and bioprinting. *Cell Tissue Res.* **2023**, *394*, 75–91. [CrossRef] [PubMed]

Disclaimer/Publisher's Note: The statements, opinions and data contained in all publications are solely those of the individual author(s) and contributor(s) and not of MDPI and/or the editor(s). MDPI and/or the editor(s) disclaim responsibility for any injury to people or property resulting from any ideas, methods, instructions or products referred to in the content.